Experimental Evidence for a Transient Tayler Instability in a Cylindrical Liquid-Metal Column

Martin Seilmayer, Frank Stefani,* Thomas Gundrum, Tom Weier, and Gunter Gerbeth
Helmholtz-Zentrum Dresden-Rossendorf, P.O. Box 510119, D-01314 Dresden, Germany

Marcus Gellert and Günther Rüdiger
Leibniz-Institut für Astrophysik Potsdam, An der Sternwarte 16, D-14482 Potsdam, Germany
(Received 9 December 2011; published 11 June 2012)

In the current-driven, kink-type Tayler instability (TI) a sufficiently strong azimuthal magnetic field becomes unstable against nonaxisymmetric perturbations. The TI has been discussed as a possible ingredient of the solar dynamo mechanism and a source of the helical structures in cosmic jets. It is also considered as a size-limiting factor for liquid metal batteries. We report on a liquid metal TI experiment using a cylindrical column of the eutectic alloy GaInSn to which electrical currents of up to 8 kA are applied. We present results of external magnetic field measurements that indicate the transient occurrence of the TI in good agreement with numerical predictions. The interference of TI with the competing large-scale convection, resulting from Joule heating, is also discussed.

DOI: 10.1103/PhysRevLett.108.244501 PACS numbers: 47.20.−k, 47.65.−d, 52.58.Lq

The last few years have seen a number of liquid metal experiments on various magnetohydrodynamic instabilities with relevance to the origin and the action of cosmic magnetic fields [1]. Dynamo action has been observed in the large-scale liquid sodium experiments in Riga, Karlsruhe, and Cadarache [2]. The helical version of the magnetorotational instability (MRI) has been evidenced in the PROMISE experiment [3], and further experiments in Maryland [4] and at Princeton [5] are devoted to the investigation of the standard version of MRI. What is missing in the liquid metal lab is any evidence of the pinch-type Tayler instability (TI) [6]. This is in remarkable contrast to the vast experience in plasma physics where the (compressible) counterpart of TI is better known as the kink instability in a z pinch [7], i.e., the limit of the Kruskal-Shafranov instability when the safety factor goes to zero. In astrophysics, TI has been discussed as a possible ingredient of an alternative, nonlinear stellar dynamo mechanism (Tayler-Spruit dynamo [8]), as a generation mechanism for helicity [9], and as a possible source of helical structures in galactic jets and outflows [10].

A particular motivation to study the TI in a liquid metal arises from the growing interest in large-scale liquid metal batteries as cheap means for the storage of highly intermittent renewable energies. Such a battery would consist of a self-assembling stratification of a heavy liquid half-metal (e.g., Bi, Sb) at the bottom, an appropriate molten salt as electrolyte in the middle, and a light alkaline or earth alkaline metal (e.g., Na, Mg) at the top. While small versions of this battery have already been tested [11], for larger versions the occurrence of TI could represent a serious problem for the integrity of the stratification. In a recent paper [12] we have proposed a simple trick to avoid the TI in liquid metal batteries by just returning the battery current through a bore in the middle. By the resulting change of the radial dependence of $B_\varphi(r)$ it is possible to prevent the condition for (ideal) TI, $\partial(rB_\varphi^2(r))/\partial r > 0$. Without such a provision, TI is expected to set in at some finite electrical current in the order of kA. The precise value is a function of various material parameters since for viscous and resistive fluids TI is known [13] to depend effectively on the Hartmann number $\mathrm{Ha} = B_\varphi R(\sigma/\rho\nu)^{1/2}$, where R is the radius of the column, σ the electrical conductivity, ρ the density, and ν the kinematic viscosity of the fluid.

In this Letter, we present experimental results that confirm the numerically determined growth rates of TI [13] as well as the corresponding prediction that the critical current increases monotonically with the radius of an inner cylinder [12,14].

The central part of our TI experiment (Fig. 1) is an insulating cylinder with a length of 75 cm and an inner diameter of 10 cm that is filled with the eutectic alloy GaInSn, which is liquid at room temperature. The physical properties of GaInSn at 25 °C are density $\rho = 6.36\times 10^3$ kg/m^3, kinematic viscosity $\nu = 3.40\times 10^{-7}$ m^2/s, and electrical conductivity $\sigma = 3.27\times 10^6$ $(\Omega\,\mathrm{m})^{-1}$. At the top and bottom, the liquid metal column is contacted by two massive copper electrodes 9 cm in height that are connected by water-cooled copper tubes to a dc power supply that can provide electrical currents of up to 8 kA. By intensively rubbing the GaInSn into the copper, we have provided good wetting, making the electrical contact as homogeneous as possible.

Although in later experiments it is planned to use ultrasonic Doppler velocimetry (UDV) in order to directly measure the axial velocity component along the z axis, for the first experiments we have decided not to use any inserts that could possibly disturb the homogeneous current going from the copper electrodes to the liquid.

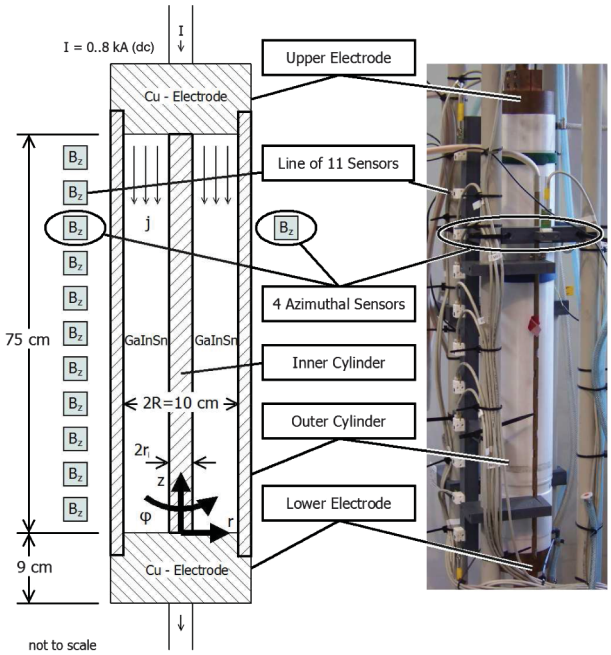

FIG. 1 (color). Experimental setup. Left: Scheme with liquid metal column and fluxgate sensors positioned along the vertical axis and the azimuth. Right: Photograph of the central part of the experiment.

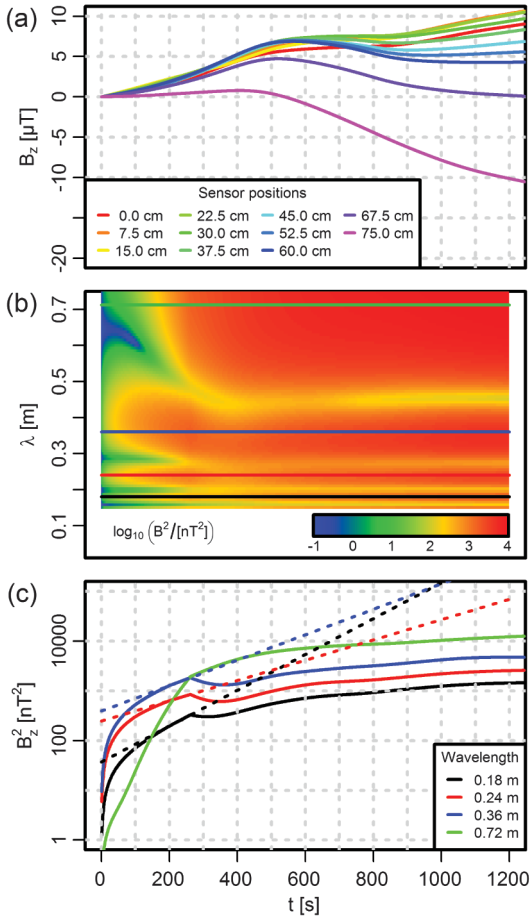

FIG. 2 (color). Magnetic fields measured along the vertical axis, for $r_i = 12.5$ mm and $I = 7$ kA. (a) Time dependence of B_z at the 11 fluxgate sensors. (b) Power spectral density dependent on time and wavelength. Note the dominance of short wavelength signals in the initial phase, and the dominance of the long wavelength signal at later times. (c) Detailed time evolution of the PSD for four significant wavelengths, showing a transition to an exponential growth around $t \sim 150$ s, which is later stopped at $t \sim 280$ s. The dashed, tangent lines indicate the growth of the short wavelength modes.

Therefore, for the identification of TI we exclusively rely on 14 external fluxgate sensors that measure the vertical component B_z of the magnetic field. Of these sensors 11 are aligned along the vertical axis (with a spacing of 7.5 cm) while the remaining 3 sensors are positioned along the azimuth in the upper part, approximately 15 cm from the top electrode. The distance of the sensors from the outer rim of the liquid metal column is 7.5 cm. This rather large value, which is certainly not ideal to identify small-wavelength perturbations, has been chosen in order to prevent saturation of the fluxgate sensors in the strong azimuthal field of the axial current.

The main goal of our experiment is to study the influence of the electric current through the fluid on the growth rate and on the amplitude of the magnetic field perturbations. This is done without any insert, as well as for two different radii of an inner nonconducting cylinder $r_i =$ 6 mm and 12.5 mm for which we expect a monotonic increase of the critical current.

For the particular case with $r_i = 12.5$ mm and $I =$ 7 kA, Figs. 2 and 3 illustrate the measured B_z data dependent on the vertical position and on the azimuth, respectively, and illustrate the procedure of data analysis. In both cases, the time stamp and the field values were set to zero a few seconds after the switch-on process of the current (a quasilinear ramp with 100 A/s) had been finalized. Figure 2(a) shows the subsequent evolution of B_z measured at the 11 vertical positions. Most of the data in Fig. 2(a) show a collective long-term trend, whose source might be increasing convection, but possibly also some geometric changes (e.g., by thermal expansion of constructional parts), that could influence the projection of the strongly dominant azimuthal field component on the measured z component.

Apart from this long-term trend, the data of Fig. 2(a) contain more extractable details on the vertical dependence. At every time instant we first subtract both the mean value as well as the linear trend in z direction and then compute the power spectral density (PSD) of the remaining signal by means of the Lomb-Scargle periodogram method [15,16]. The resulting PSD, dependent on time and wavelength, is shown in Fig. 2(b). At the beginning we observe the simultaneous growth of three modes with short wavelengths, but later a long-wavelength mode becomes dominant. The time dependencies of four exemplary modes with wavelengths of 18, 24, 36, and 72 cm are shown separately in Fig. 2(c). After some initial transient of about 150 s during which the fluid (having been stirred

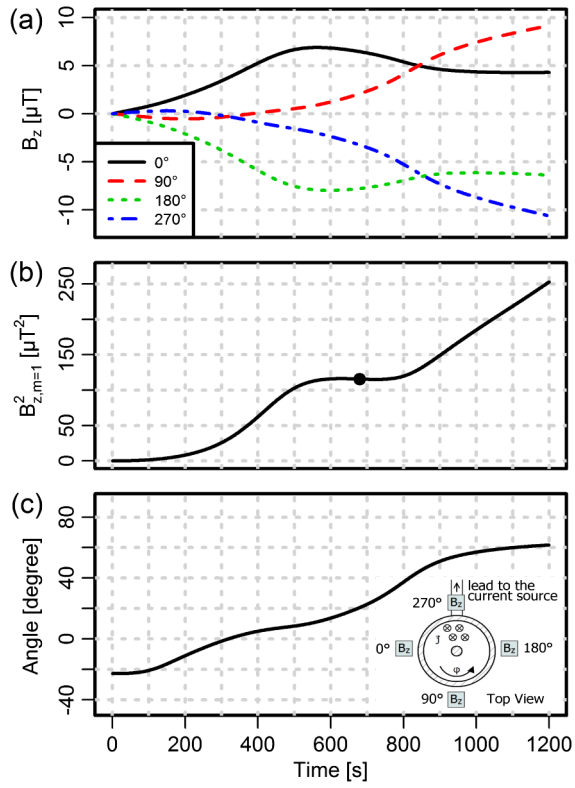

FIG. 3 (color online). Magnetic field data measured along the azimuth, for $r_i = 12.5$ mm and $I = 7$ kA. (a) Time dependence of B_z at the 4 fluxgate sensors. The $m = 1$ character is clearly visible. (b) Squared magnetic field amplitude of the $m = 1$ mode. The dot indicates the inflection point. (c) Angle of the $m = 1$ mode.

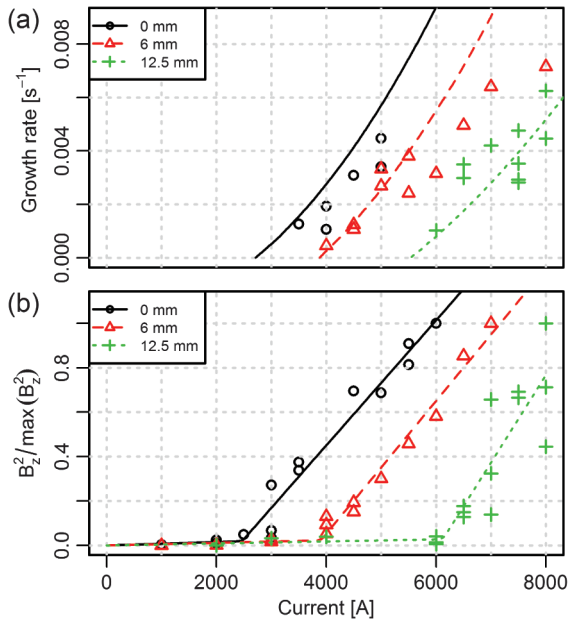

FIG. 4 (color). (a) Measured growth rates (markers) and their numerical predictions (lines) for three different radii of the inner cylinder, dependent on the current. (b) Measured squared magnetic field strength (markers) of the $m = 1$ mode, and their piecewise linear fits (lines). The maximum squared fields for $r_i = 0$, 6, and 12.5 mm are 61.0, 543.3, and 1668.1 μT^2, respectively.

by the switch-on process) is calmed down, the growth of all short-wavelength modes acquires an exponential character, and we can read off the corresponding growth rates in the time interval between 200 and 280 s [see the dotted lines in Fig. 2(c)]. The similarity of the growth rates of the short-wavelength modes might indicate a merging of neighboring cells as it is also observed in (preliminary) numerical simulations of the combined action of TI and thermal convection.

This regular exponential growth of the short-wavelength modes stops suddenly at $t = 280$ s, when the long-wavelength mode (here with a wavelength of 72 cm) becomes dominant. Interestingly, the growth rate of this 72 cm mode after the transition becomes quite similar to the growth rate of the 36 cm mode shortly before the transition. This may indicate a sudden doubling of the wavelength with increasing temperature and convection. Though not shown here, below 6 kA the convection dominates from the very beginning, and there are no signs of any corresponding transition from short- to long-wavelength modes.

Now we turn to the discussion of the azimuthal dependence of the induced B_z perturbations, as measured by the four sensors around the cylinder. The behavior shown in Fig. 3(a) clearly indicates a nonaxisymmetric ($m = 1$) mode of the field with a growing amplitude at the beginning and some rotation and further growth at later times. The time evolution of the squared amplitude $[B_z(0°) - B_z(180°)]^2 + [B_z(90°) - B_z(270°)]^2$ of this $m = 1$ mode is presented in Fig. 3(b), and its corresponding angle in Fig. 3(c).

In Fig. 4 we compile the dependence of various quantities on the radius of the inner cylinder and on the current through the fluid. First, in Fig. 4(a), we compare the growth rate of the 18-cm mode, as extracted from the periods with clear exponential growth [see Fig. 2(c) for one example] with the numerical growth rates predicted [13] for the mode with optimum wavelength (approximately 13 cm). Despite some scatter of the data, we observe a quite reasonable agreement with the numerical predictions.

The second quantity of interest is the saturation level of the magnetic field. Similar to many other instabilities, for TI one would expect a more or less linear behavior of the saturated squared magnetic field above the critical current, according to $B^2 \sim (I - I_{\mathrm{crit}})$. However, the specific problem of our liquid metal experiment is that the saturation of the TI does not rely on an *intrinsic* backreaction process, but on the *extrinsic* stabilizing effect of the increasing large-scale convection. With this caveat in mind, in Fig. 4(b) we try to identify the critical current by plotting the squared magnetic field of the $m = 1$ mode at the inflection point of the corresponding curves [indicated, for this example, by the point in Fig. 3(b)].

Starting at this inflection point we typically also observe a move of the angle of the field pattern to a new value.

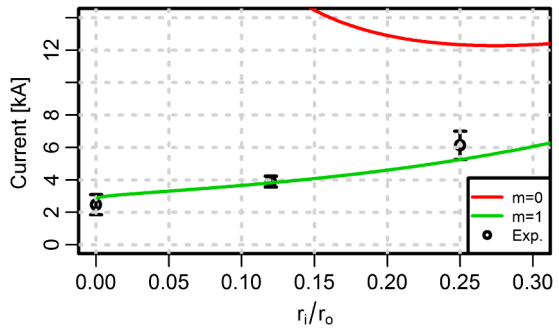

FIG. 5 (color online). Comparison of the determined critical currents with the numerical predictions for the $m = 1$ mode. The numerical prediction for the $m = 0$ (sausage) mode is indicated partly.

We hypothesize that this "mode locking" starts when the long-wavelength mode becomes dominant and aligns to some preferred azimuthal direction (determined, e.g., by slight geometric imperfections of the experimental setup). The observed magnetic field level at this inflection point is thus yet determined by the TI alone. It is reasonable to assume a monotonic, if not linear, dependence of the quadratic field strength (taken at the inflection point) on $(I - I_{\mathrm{crit}})$ to characterize the TI.

By applying a piecewise linear fit to the observed squared field intensities [see Fig. 4(b)], we can determine the critical current at the crossing point of the two straight lines. Figure 5 shows the critical currents determined that way and the error bars (with a 95% confidence level) in comparison with the numerically determined ones [13]. Despite the fact that the inflection-point criterion for the determination of the saturated magnetic field strength is certainly debatable, we again obtain a reasonable correspondence with the predicted critical currents.

The investigation of a current-driven instability in a column of a liquid metal has revealed a rather complex behavior, comprising (after some initial transient) an exponential growth of the anticipated TI mode followed by a large-scale convection dominated by Joule heating. From the sharp bends of the amplitude evolution of the short-wavelength modes [see Fig. 2(c)] it becomes apparent that the growing intensity of convection limits the further growth of the TI. This is a drawback of the present experimental configuration since it prevents any investigation of the *intrinsic* saturation mechanism of TI. This mechanism is thought to rely on the TI-triggered onset of turbulence leading to an enhanced (turbulent) resistivity (β effect, see [17]). While a homogeneous distribution of the turbulent resistivity could already lead to the saturation of TI through a decrease of the effective Hartmann number (at fixed current), a radial variation of it could be an even more efficient saturation mechanism by virtue of changing the current distribution in radial direction. Up to present, however, voltage measurements between the copper electrodes have shown no evidence of any β effect. Therefore, the investigation of this interesting saturation mechanism would require a significant weakening of the role of Joule heating by using a heat conducting outer cylinder, by choosing a horizontal orientation of the column (which, however, introduces an explicit symmetry breaking), or by increasing the radius, and/or by replacing GaInSn with liquid sodium, for which TI is expected to occur already around 1 kA. Such a large-scale sodium experiment, in which TI and MRI can be studied together, is planned for the future.

This work was supported by DFG in frame of SFB 609 and SPP 1488, and by the Energy Storage Initiative of the Helmholtz society. Fruitful discussions with Rainer Arlt, Rainer Hollerbach, and Manfred Schultz are gratefully acknowledged. We thank Bernd Nowak and Thomas Wondrak for technical support.

*F.Stefani@hzdr.de

[1] F. Stefani, A. Gailitis, and G. Gerbeth, Z. Angew. Math. Mech. **88**, 930 (2008).
[2] A. Gailitis *et al.*, Phys. Rev. Lett. **84**, 4365 (2000); R. Stieglitz and U. Müller, Phys. Fluids **13**, 561 (2001).R. Monchaux *et al.*, Phys. Rev. Lett. **98**, 044502 (2007).
[3] F. Stefani, T. Gundrum, G. Gerbeth, G. Rüdiger, M. Schultz, J. Szklarski, and R. Hollerbach, Phys. Rev. Lett. **97**, 184502 (2006); F. Stefani, G. Gerbeth, T. Gundrum, R. Hollerbach, J. PriedeG. Rüdiger, and J. Szklarski, and Phys. Rev. E **80**, 066303 (2009).
[4] D. R. Sisan, N. Mujica, W. A. Tillotson, Y. M. Huang, W. Dorland, A. B. Hassam, T. M. Antonsen, and D. P. Lathrop, Phys. Rev. Lett. **93**, 114502 (2004).
[5] M. D. Nornberg, H. Ji, E. Schartman, A. Roach, and J. Goodman, Phys. Rev. Lett. **104**, 074501 (2010).
[6] R. J. Tayler, Mon. Not. R. Astron. Soc. **161**, 365 (1973); Yu. V. Vandakurov, Sov. Astron. **16**, 265 (1972).
[7] W. F. Bergerson, C. B. Forest, G. Fiksel, D. A. Hannum, R. Kendrick, J. S. Sarff, and S. Stambler, Phys. Rev. Lett. **96**, 015004 (2006).
[8] H. C. Spruit, Astron. Astrophys. **381**, 923 (2002).
[9] M. Gellert, G. Rüdiger, and R. Hollerbach, Mon. Not. R. Astron. Soc. **414**, 2696 (2011).
[10] R. Moll, H. C. Spruit, and M. Obergaulinger, Astron. Astrophys. **492**, 621 (2008).
[11] R. D. Weaver, S. W. Smith, and N. L. Willmann, J. Electrochem. Soc. **109**, 653 (1962); D. J. Bradwell, H. Kim, A. H. C. Sirk, and D. R. Sadoway, J. Am. Chem. Soc. **134**, 1895 (2012).
[12] F. Stefani, T. Weier, Th. Gundrum, and G. Gerbeth, Energy Conv. Manag. **52**, 2982 (2011).
[13] G. Rüdiger, M. Schultz, and M. Gellert, Astron. Nachr. **332**, 17 (2011).
[14] G. Rüdiger and M. Schultz, Astron. Nachr. **331**, 121 (2010).
[15] N. R. Lomb, Astrophys. Space Sci. **39**, 447 (1976); J. D. Scargle, Astrophys. J. **263**, 835 (1982).
[16] See Supplemental Material at http://link.aps.org/supplemental/10.1103/PhysRevLett.108.244501 for a brief description of the Lomb-Scargle algorithm.
[17] M. Gellert and G. Rüdiger, Phys. Rev. E **80**, 046314 (2009).